Int. J. Heat Mass Transfer. Vol. 37, No. 2, pp. 207–215, 1994
Printed in Great Britain

0017–9310/94 $6.00 + 0.00

Forced convection heat transfer with phase-change-material slurries: turbulent flow in a circular tube

EUNSOO CHOI, YOUNG I. CHO and HAROLD G. LORSCH
Department of Mechanical Engineering and Mechanics, Drexel University, Philadelphia, PA 19104, U.S.A.

(*Received* 5 *January* 1993 *and in final form* 27 *July* 1993)

Abstract—The present study investigates the increase in the convective heat transfer coefficient as well as the increase in the thermal capacity of a working fluid by using the latent heat from a solid–liquid phase change of particles. A long heating test section (627 diameters) with a uniform heat flux boundary condition is constructed in order to study the effects of the phase-change phenomenon produced by a phase-change-material (PCM)—water slurry on the convective heat transfer coefficient in a turbulent flow. The study introduces a method to generate very fine PCM particles inside a flow loop using an emulsifier. With such fine PCM particles, the flow loop did not clog. Local pressure drops and local heat transfer coefficients are measured along the test section. The pressure drop significantly decreased at the point where the PCM particles in the slurry melted. The local convective heat transfer coefficient was found to vary significantly when the particles melted. This made it difficult to apply the LMTD method to the analysis of the PCM slurry flow heat transfer. The study proposes a new three-region melting model, and provides an explanation of the physical mechanism of the convective heat transfer enhancement due to the PCM particles.

INTRODUCTION

THE OBJECTIVE of the present study is to investigate the feasibility of using phase-change materials (PCM) to enhance the convective heat transfer in district cooling systems. A conventional chilled-water system requires a high volumetric flow rate, and as a result consumes a large amount of pumping power. The present study attempts to increase the convective heat transfer coefficient by increasing the effective thermal capacity of working fluids, a technique that would permit the use of a smaller volumetric flow rate and smaller heat exchangers. The major challenge in applying liquid–solid phase-change materials to a convective heat transfer is how to circulate the phase-change material continuously through the heat transfer flow loop.

One of the earlier liquid–solid phase-change systems tried was an ice–water slurry. In this method, fine ice particles were generated in the cooling plant and circulated with cold water. Cleary *et al.* [1] performed an experiment with the ice–water slurry and found that a 25% ice slurry had a thermal capacity that was two to four times higher than chilled water. They generated very fine ice particles (0.1 to 0.2 mm) in a 6% glycol–water solution and successfully circulated the ice slurry through hydraulic and thermal test sections. The hydraulic test section consisted of smooth copper pipes of 25 mm and 50 mm ID with a total length of 15 m. The thermal test section included two heat exchangers, a small plate heat exchanger, and a shell-and-tube heat exchanger. The ice slurry circulating on one side of the heat exchanger was melted by hot water circulating on the other side.

As the concentration of ice particles in the ice-slurry mixture increased up to 30%, the researchers reported no significant change in the friction factor compared to pure water. The log-mean-temperature-difference (LMTD) method was used to calculate an overall heat transfer coefficient, which was slightly higher for the ice slurry than for pure water. A doubling or tripling of the ice particle concentration was found to produce a small effect on the convective heat transfer coefficient. It is still not known why Cleary *et al.* obtained a small enhancement of the heat transfer coefficient. Furthermore, the validity of the LMTD method to calculate the heat transfer coefficient of the ice slurry was not clearly presented.

Another method of generating small ice particles, called 'direct freeze', was tested by Winters [2]. Water was mixed with a liquid refrigerant at a pressure below the saturation pressure of the refrigerant. As the refrigerant evaporated, water solidified to small ice particles of 1 to 2 mm diameter, which were then suspended in cold water and circulated through a flow loop. However, the ice slurry failed to circulate through a plate heat exchanger because of ice blockage, especially at T-junctions. The pressure drop over circular pipes of 2-, 4-, and 6-inch ID for the ice-slurry was reported to be almost the same as for pure water.

A slurry using phase-change materials is similar to the ice slurry, since ice is just one kind of phase-change material. If phase-change materials can be suspended as small solid particles in a carrier fluid and circulated through a heat exchanger, the thermal capacity and the heat transfer coefficient of the carrier fluid can be increased, provided that the phase-change temperature is in the temperature range of the heat

NOMENCLATURE

C	specific heat
$\bar{C}$	average specific heat of a mixture
D	internal diameter of test section
h	convective heat transfer coefficient
k	thermal conductivity
L	total length of heating test section or length of each melting region
$\dot{m}$	mass flow rate
Nu	Nusselt number, hd/k
Pr	Prandtl number, v/α
P	pressure
ΔP	pressure difference
$\dot{Q}$	heating rate
Q_v	volumetric flow rate
Re	Reynolds number, $\rho Vd/\mu$
T	temperature
ΔT	temperature difference between inlet and outlet fluid
U	overall heat transfer coefficient
V	mean velocity
x	axial distance from the starting point of the heating test section.

Greek symbols

α	thermal diffusivity, $k/(\rho C)$
λ	heat of fusion
μ	dynamic viscosity
v	kinematic viscosity, μ/ρ
ρ	density
ϕ	volumetric loading fraction of PCM.

Subscripts

1	region I
2	region II
3	region III
b	value of bulk mean temperature
bi	value of inlet bulk mean temperature
c1	inlet of cold fluid in heat exchanger
c2	outlet of cold fluid in heat exchanger
cf	cold fluid in heat exchanger
d	internal diameter of test section
eff	effective value
h1	inlet of hot fluid in heat exchanger
h2	outlet of hot fluid in heat exchanger
hx	hexadecane
hf	hot fluid in heat exchanger
hl	liquid hexadecane
hs	solid hexadecane
m	melting point
pc	with phase change
s	single phase
wt	water.

exchanger. There are many kinds of phase-change materials with different melting temperatures [3] to make this choice possible.

Kasza and Chen [4] suggested a microencapsulated phase-change-material (PCM) slurry as a working fluid in forced convection heat transfer, and outlined its potential benefits. The microencapsulation technique uses hollow spheres smaller than 1 mm in diameter to encapsulate a phase-change material. They claimed that, if these small spheres were suspended in a carrier fluid and circulated through the heating test section, the convective heat transfer coefficient would increase because of the increases in the effective thermal conductivity, k_{eff}, and the effective thermal capacity, C_{eff}.

One of the correlations describing the convective heat transfer coefficient for heating in a fully developed turbulent flow of a single fluid [5] is

$$Nu_d = 0.0395\, Re_d^{3/4}\, Pr^{1/3}. \quad (1)$$

Therefore, the convective heat transfer can be expressed in terms of the thermal conductivity and the thermal capacity as

$$h \sim k^{2/3} C^{1/3}.$$

According to Sohn and Chen [6, 7], the effective thermal conductivity of a liquid–solid suspension is larger than that of a pure liquid, a phenomenon that was attributed to the microconvection around solid particles, which results in an increased convective heat transfer coefficient. For example, a thirty-fold increase in the effective thermal conductivity and a ten-fold increase in the heat transfer coefficient were predicted for a 30% suspension of 1 mm particles in a 10 mm diameter pipe at an average velocity of 10 m s^{-1} [4]. It is of note that in a real industrial application, it is very difficult to circulate the 30% suspension of 1 mm particles through a 10 mm diameter pipe without clogging. Furthermore, if the suspended particles are smaller than 0.1 mm, the microconvection effect will be very small.

The effect of the latent heat of a phase-change material on the heat transfer coefficient was represented by Kasza and Chen [4] as

$$\frac{h_{\text{pc}}}{h_{\text{s}}} = \left(\frac{\phi\lambda}{C\Delta T}\right)^{1/3}, \quad \text{for } \phi\lambda \gg C\Delta T. \quad (2)$$

Colvin *et al.* [8] defined the effective heat capacity as

$$C_{\text{eff}} = \bar{C} + \frac{\phi\lambda}{\Delta T} \quad (3)$$

which included the effect of sensible heat of the

mixture. By using equation (3), equation (2) can be modified to

$$\frac{h_{pc}}{h_s} = \left(\frac{\bar{C}+\phi\lambda/\Delta T}{C}\right)^{1/3}. \quad (4)$$

Colvin *et al.* [8] also developed a manufacturing technology to produce very small encapsulated phase-change materials. They applied these encapsulated phase-change materials in a convective heat transfer test section and claimed a 50–100% higher heat transfer coefficient.

Based on previous research, Charunyakorn *et al.* [9, 10] tried to develop a numerical simulation of the laminar flow with a phase-change slurry. The slurry temperature at the inlet of the heating test section was assumed to be the melting temperature of the particles. The local Nusselt number was maximum at the inlet of the heating test section and decreased along the flow direction, a trend which was the same as for the single-phase flow. However, the Nusselt number of the phase-change-slurry flow was 2–4 times higher than that of the single-phase flow.

Roy and Sengupta [11] tested the properties and stability of microencapsulated phase-change materials. Three different microcapsules (i.e. 50, 100, and 250 μm) with two different wall thicknesses (i.e. 15 and 30%, where the wall thickness was represented as the volumetric fraction of the wall to the whole capsule volume) were tested through 10 to 100 thermal cycles. The microcapsules with thin walls (i.e. 15%) were unable to withstand the thermal cycles, while those with thick walls (i.e. 30%) were found to be stable both structurally as well as thermally.

Since the production of very fine microencapsulated phase-change materials is proprietary [12, 13] and still expensive, it does not seem feasible in the near future to apply this method to district cooling systems, where a large amount of working fluid is required. Choi *et al.* [14] has developed a new inexpensive technology to produce phase-change-material particles smaller than 0.1 mm in diameter by using an emulsifier; this method is used in the present research.

EXPERIMENTAL APPARATUS

Figure 1 shows the schematic diagram of the experimental apparatus, which consists of two reservoir tanks (one for the carrier fluid and the other for the liquid phase-change material), a surge tank, two pumps, two flow meters, two static mixers, a constant-temperature circulating bath, a cooling bath, a hydrodynamic entry section, a main heat transfer test section, a collecting reservoir, and a DC power supply. The test section was made up of nominal 0.9525 cm stainless steel tubing. Its inside diameter was measured by filling the tube with water and measuring the mass of the filled water, and it was found to be 1.016 cm.

The test section was composed of a hydrodynamic entry section and a heating test section. The hydrodynamic entry section was long enough (325 diameters) not only to produce a fully-developed flow at the start of the heating test section but also to measure fully-developed pressure drops in the suspension flow without heating behind the heating test section. The length of the thermal entrance region for single-phase turbulent flow was approximately 15–20 diameters [15–17]. The length of the main heating test section was approximately 627 diameters, a distance that was long enough to capture the phase-change phenomena

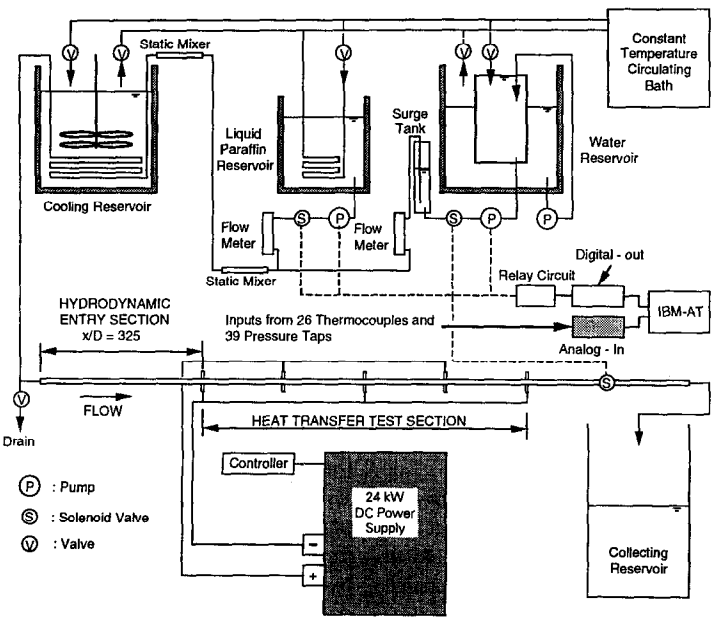

FIG. 1. Schematic diagram of experimental apparatus.

in a two-phase flow test. The entire length of the test section including the entry section was approximately 10 m.

The water bath was composed of dual containers. Water was pumped from the outside container to the inside container, and overflowed from the top of the inside container to the outside container in order to maintain a constant head. The temperature of the water bath was controlled by a constant-temperature circulating bath at approximately 17°C, which was slightly higher than the melting temperature of 16.5°C for commercial grade hexadecane. A proper amount of emulsifier [14] was mixed with the water in its reservoir. The liquid phase-change-material reservoir was filled with liquid hexadecane, and its temperature was set at approximately 20°C, i.e. room temperature.

The flow rates of the water and the liquid hexadecane were varied by two separate pumps; they were measured by two separate rotameters, which were calibrated by direct weighing for various flow rates and temperatures. A surge tank was installed between the water pump and the water-side rotameter to suppress fluctuations from the pump. In normal working conditions, the flow loop was pressurized at approximately 172 kPa (25 psig). The cooling bath was composed of a controlled-speed stirrer and a cooling coil. A large quantity of ice and water was put in the cooling bath. The temperature of the cooling bath was controlled at approximately 3°C.

Water from the inside container of the water bath was mixed with liquid hexadecane in the static mixer, where water and hexadecane became an emulsion (i.e. liquid–liquid mixture); this mixture was circulated through the cooling coil in the cooling bath, where the fine liquid hexadecane particles solidified into fine solid particles. The temperature of this mixture of water and solid hexadecane in suspension was maintained at approximately 7–8°C at the exit of the cooling coil. This was much lower than the melting temperature of the hexadecane, which ensured the solidification of the hexadecane particles.

The size of solid hexadecane particles generated depended on the concentration of the emulsifier [13], and was smaller than 0.1 mm. Those small particles neither stuck to the surface of the cooling coil nor grew in size; thus, clogging did not occur. The suspension was sampled before the beginning of the test section through a faucet, and the size and homogeneity of the particles were constantly monitored during the test. It is of note that the above particle generating system did not need any particle feeding facility. The volumetric fraction of the particles could be determined accurately by independently measuring the flow rates of water and liquid hexadecane.

A high-current DC power supply was used to heat the stainless steel tubing. The heating test section was electrically divided into four zones and connected in parallel, in order to match the required electrical resistance of the power supply. Nineteen pressure taps were installed along the test section at 50 diameter intervals. Holes of 0.0794 cm diameter were drilled through the stainless steel tube wall. The pressure was measured differentially over every two adjacent pressure taps by using two fluid switch wafers (Scanivalves). This allowed all the pressure measurements to be in a similar range and thus increased the measuring accuracy. A pressure transducer (Validyne DP103-18) with a 0.5 psi diaphragm was calibrated by water columns and used to measure pressure drops. Thermocouples were calibrated by ice point and steam point of distilled water before they were attached to the test section. Calibration results are given elsewhere [18].

Three solenoid valves, at the water inlet, the water outlet, and the liquid phase-change-material inlet, respectively, were controlled by a relay circuit connected to an IBM PC. All the temperature and pressure data were recorded directly into the IBM PC through a 16-channel, 16-bit high-resolution Omega data acquisition system.

RESULTS AND DISCUSSIONS

Accuracy of measurements

At first, water was circulated to check the overall accuracy of measurements. The energy balance ratio, which was defined as the ratio of the thermal energy removed by water to the electrical energy supplied by the power supply, was within 2% of unity. The average deviation of the measured Fanning friction coefficients from the predicted values of the Blasius equation [19] was 2.1%. The measured local Nusselt number corrected by a radial viscosity change effect [15, 16, 20] was between the two values predicted by the Dittus–Boelter correlation [21] and the Petukhov correlation [20]. The details of the above results are given elsewhere [18].

Pressure drop measurements with PCM–water mixture

Tests were conducted with water (0% hexadecane) and a 10% mixture of hexadecane in water. The percentage of hexadecane was calculated based on the volumetric fraction of hexadecane in the hexadecane–water mixture. At first, water was circulated through the test section, and then the hexadecane–water mixture was circulated at the same volumetric flow rate. The Reynolds number at the inlet of the heating test section was 13 230 for the water test. When hexadecane was mixed with water, the hexadecane–water mixture was an emulsion (i.e. a mixture of liquid hexadecane and water) prior to entering the cooling bath. When the temperature of the cooling bath was set at a higher temperature than the melting temperature of hexadecane, the emulsion mixture was circulated through the test section. When the cooling bath was set at a lower temperature than the melting temperature of hexadecane, liquid particles of hexadecane in the emulsion solidified at the exit of the cooling bath, and a suspension (i.e. a mixture of solid hexadecane particles and water) mixture was circulated through the test section. The suspended particles

melted in the heating test section, and the suspension returned to an emulsion at the end of the heating test section.

Local static pressures were measured for water, for 10% emulsion, and for 10% suspension, as shown in Fig. 2. Figure 2(A) shows local static pressure changes along the test section from $x/D = -300$ to $x/D = 600$. The heating test section started at $x/D = 0$. There was no significant change in local pressure profiles between water and the 10% hexadecane emulsion, but a noticeable change occurred for the 10% suspension. Figure 2(B) shows local differential pressures measured over 50-diameter distances along the test section. The local differential pressures of water were almost identical to those of the 10% hexadecane emulsion along the entire test section. The local differential pressures of the 10% hexadecane suspension were much higher than those of the emulsion and started to drop suddenly at $x/D = 370$ to the level of the emulsion. The local differential pressures of the suspension were found to be approximately 13% higher than those of the emulsion before the melting region (i.e. $x/D < 370$). This sudden change in the differential pressure could be used to address the melting phenomenon of the suspension in the heat transfer test section, as will be shown later.

Figure 2(B) further indicates that the differential pressure decreased over a relatively short region, which means that the suspension melted over that short region in the heat transfer test section. The bulk mean temperature of the suspension at the inlet of the heating test section was lower than the melting temperature of hexadecane, and increased along the heating test section. Until the bulk mean temperature of the suspension reached the melting temperature of hexadecane, almost all the solid hexadecane particles in the suspension are believed to remain solid, as manifested by the higher pressure drops even though the wall temperature was much higher than the melting temperature of hexadecane.

When the heating rate increased, the onset of the melting region moved further upstream. Ten-percent hexadecane suspensions were heated at three different heating rates (i.e. 2.98, 6.32, and 12.22 kW); the measured local pressures and the corresponding local differential pressures are shown in Figs. 3(A) and (B), respectively. The particles in the suspension were not melted with the heating rate of 2.98 kW, since there was no sudden change in the pressure drop measurements along the test section (see open circles in Fig. 3(B)). The particles at the outlet of the test section were observed to be almost solid. When the heating rate increased to 6.32 kW, the melting region started at $x/D = 370$, while it started at $x/D = 250$ when the heating rate was 12.22 kW.

Bulk mean temperature with PCM–water mixture

The estimation or measurement of local bulk mean temperatures is necessary if one wants to calculate the local Nusselt number. For single-phase flow, the local bulk mean temperature can easily be estimated from a linear interpolation of inlet and outlet fluid temperatures. Unlike for the single-phase flow, it is extremely challenging to find the local bulk mean temperature for a two-phase flow. Traditionally, in order to determine the local Nusselt number, outer wall temperatures of the heating test section were measured, from which inner wall temperatures were

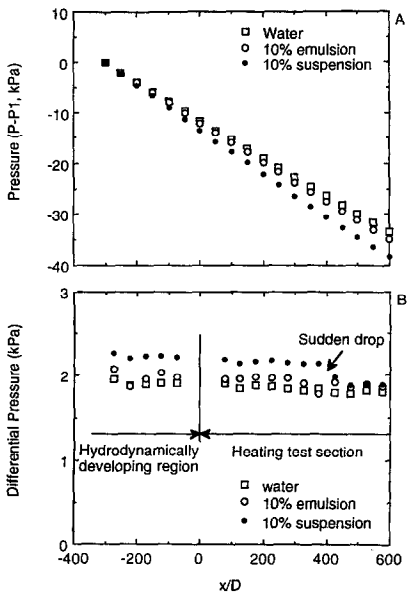

FIG. 2. Pressure profiles of water, 10% emulsion, and 10% suspension mixtures with heating rates of 6.29, 6.21, and 6.32 kW, respectively.

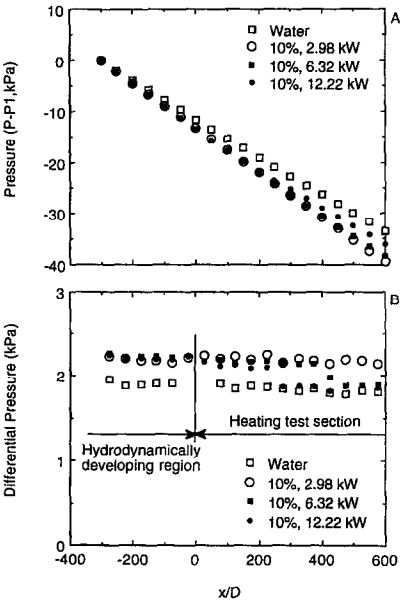

FIG. 3. Pressure profiles of water and 10% suspension mixtures with heating rates of 2.98, 6.32, and 12.22 kW, respectively.

calculated by a heat conduction equation with a uniform heat source in the wall.

The present study proposes a new three-region melting model to determine the local bulk mean temperatures for a PCM–water mixture. The model uses three different energy balance equations in three regions, as shown in Fig. 4. Region I extends from the inlet of the heating test section to the onset of melting, where hexadecane particles in the mixture were solid particles, and thus the thermal capacity of solid hexadecane should be used in the energy balance equation. Region II is where solid hexadecane particles melt, and thus the bulk mean temperature of the mixture is assumed to be the melting temperature of hexadecane. Region III extends from the point of the completion of melting to the outlet of the heating test section, and thus the thermal capacity of liquid hexadecane should be used in the energy balance equation.

Using this three-region melting model, the bulk mean temperature profile was determined along the heating test section as depicted in Fig. 4. In Region I, the mean temperature increases linearly, and the slope of the straight line is predictable by the thermal capacities of water and solid PCM. After the mean temperature reaches the melting temperature of the PCM, it remains constant until all the PCM particles are melted. In Region III, the mean temperature increases again linearly with a slope that is predictable by the thermal capacities of water and liquid PCM. When the particle size is small enough and there is a good mixing by the turbulence of the flow, the three-region melting model is physically valid.

Table 1 represents the derived equations for the determination of the length of each region and the associated bulk mean temperature profile, $T_b(x)$. In order to use these equations, one needs to know the properties of PCM. Choi *et al.* [22] performed a thermal analysis of laboratory and commercial grades of hexadecane and tetradecane. Commercial-grade values are more important than laboratory-grade values because laboratory-grade chemicals could not be used in an industrial application due to their high cost. Table 2 lists the thermo–physical properties of hexadecane.

Ten-percent hexadecane–water suspension mixtures were tested with two different heating rates (6.21 and 12.22 kW). Figure 5 compares measured local differential pressures and calculated bulk mean temperatures from the three-region melting model. Where the measured differential pressures showed a sudden drop, the bulk mean temperature also suddenly changed, indicating the onset of Region II. In other words, the sudden drop in the measured differential pressure occurred at the point where the bulk mean temperature reached the melting temperature of hexadecane. Furthermore, where the differential pressure again reached an asymptotic level, the bulk mean temperature began to rise, indicating that all the solid hexadecane particles had completely melted, and a liquid hexadecane–water mixture had been achieved. The comparison between the measured differential pressure and the calculated bulk mean temperature supports the validity of the proposed three-region melting model.

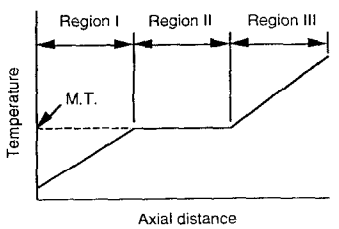

FIG. 4. Three-region melting model for the bulk mean temperature of the PCM-water mixture (M.T. represents the melting temperature of PCM).

Table 1. Derived bulk mean temperature profile equation and length of each region

Region I:

$$T_b(x) = T_{bi} + \frac{\dot{Q}}{\rho_{wl}(1-\phi)Q_v C_{wl} + \rho_{hl}\phi Q_v C_{hs}} \frac{x}{L}$$

$$\frac{L_1}{L} = \frac{[\rho_{wl}(1-\phi)Q_v C_{wl} + \rho_{hl}\phi Q_v C_{hs}](T_m - T_{bi})}{\dot{Q}}$$

Region II:

$$T_b(x) = T_m$$

$$\frac{L_2}{L} = \frac{\rho_{hl}\phi Q_v \lambda}{\dot{Q}}$$

Region III:

$$T_b(x) = T_m + \frac{\dot{Q}}{\rho_{wl}(1-\phi)Q_v C_{wl} + \rho_{hl}\phi Q_v C_{hl}} \left[\frac{x-(L_1+L_2)}{L}\right]$$

$$\frac{L_3}{L} = 1 - \frac{L_1+L_2}{L}$$

Convective heat transfer coefficient measurements with PCM–water mixture

A test was conducted with a 10% hexadecane–water suspension mixture at a 12.30 kW heating rate; Fig.

Table 2. Properties of hexadecane

Properties		Values	Units
Heat capacity	C_{hl}†	2190	J kg^{-1} C^{-1}
	C_{hs}‡	1650	J kg^{-1} C^{-1}
Density	ρ_{hl}	773.3	kg m^{-3}
Viscosity	μ_{hl}	0.00334	kg m^{-1} s^{-1}
Thermal conductivity	k_{hl}	0.144	W m^{-1} C^{-1}
Prandtl number	Pr_{hl}	50.80	
Heat of fusion	λ_{hx}	224–185§	J g^{-1}
Melting temperature	T_m	17.2–12.1§	C

† Heat capacity of the liquid hexadecane.
‡ Heat capacity of the solid hexadecane.
§ Measured values from laboratory to commercial grade: the higher values are for laboratory grade.

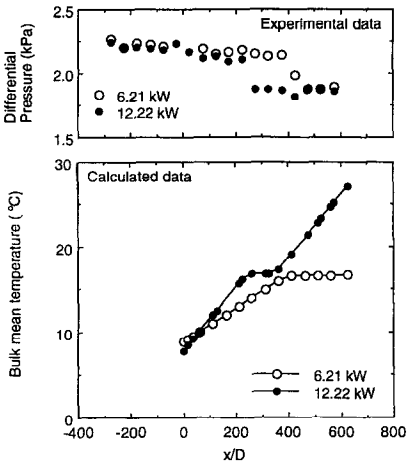

FIG. 5. Measured pressure drops and bulk mean temperature profiles according to the three-region melting model for two different heating rates.

6 compares the local convective heat transfer coefficients with the calculated bulk mean temperature curve. Along the test section, the heat transfer coefficient was found to increase in Region I, to decrease in Region II, and to increase again in Region III.

In order to explain this phenomenon, Fig. 7 shows a flow structure for a two-phase PCM mixture flow. We speculate that in Region I, a very thin layer of melted particles existed near the wall because the wall temperature was higher than the melting temperature of hexadecane, even though the bulk mean temperature was lower than the melting temperature. In order to support this, consider two particles, A and B, as shown in Fig. 7. When both particles hit the wall, particle B would have a greater possibility to melt than particle A, for the following reasons: (1)

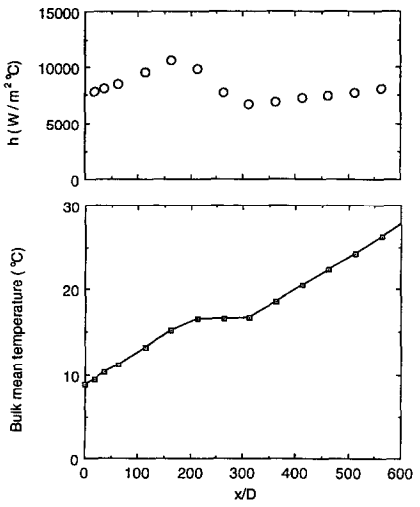

FIG. 6. Measured local convective heat transfer coefficients and bulk mean temperatures of 10% hexadecane–water suspension mixture with heating rate of 12.30 kW.

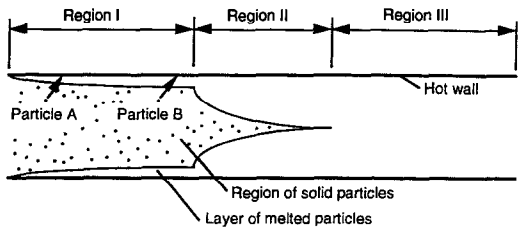

FIG. 7. Schematic diagram of the postulated suspension melting process.

the bulk mean temperature and wall temperature increased along the axial direction; (2) the temperature of particle B was closer to the melting temperature than that of particle A; and (3) the wall temperature near particle B was higher than that near particle A. As more particles melted, the heat transfer coefficient would increase.

The thickness of the melted layer increased abruptly in Region II because the bulk mean temperature reached the melting temperature of hexadecane. The increased thickness of this layer prevented the transport of solid particles to the wall. Moreover, the number of solid particles decreased substantially, resulting in a decreasing heat transfer coefficient along the flow direction in Region II. No more solid particles exist in Region III. Because the bulk mean temperature of the mixture increased along the flow direction, the viscosity decreased and the local Reynolds number increased, resulting in a slightly increasing heat transfer coefficient.

In Fig. 8, the measured convective heat transfer coefficients of the hexadecane–water mixtures with two different heating rates (i.e. 12.30 and 6.21 kW) are compared with those of water. The volumetric flow rates of the 10% hexadecane mixtures were approximately the same as that of water. The Reynolds number for the water run was 13 230 at the inlet of the heating test section and increased to 17 490 at the outlet, which was due to the decrease in water

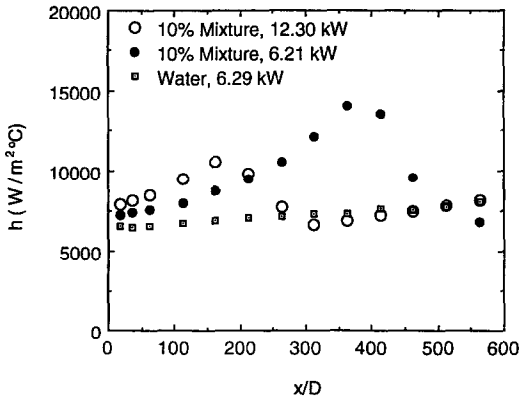

FIG. 8. Heat transfer coefficient comparison for the same volumetric flow rates. Reynolds number was 13 225–17 493 for the case of water.

viscosity caused by the bulk-mean-temperature increase.

The local convective heat transfer coefficient of the 10% mixtures reached a maximum value at $x/D = 370$ for a heating rate of 6.21 kW, and at $x/D = 160$ for a heating rate of 12.30 kW. Those positions of the maximum convective heat transfer coefficients coincided with the starting positions of the melting regions shown in Fig. 3(B). The maximum and average convective heat transfer coefficients of the 10% mixture with a heating rate of 12.30 kW were found to be lower than those with a heating rate of 6.21 kW. Colvin *et al.* [8] also reported similar effects of heating rates on the average heat transfer coefficient. We speculate that, when the heating rate was very high, the melted layer near the wall became thick, preventing the radial migration of solid particles from the center to the wall, resulting in a lower convective heat transfer coefficient.

Discussions on the LMTD method and the effective thermal capacity

In order to obtain convective heat transfer coefficients for an ice-slurry system, Cleary *et al.* [1] used the LMTD method. In the LMTD method, the following equation

$$\frac{\mathrm{d}(T_{\mathrm{hf}}-T_{\mathrm{cf}})}{T_{\mathrm{hf}}-T_{\mathrm{cf}}} = -U\left(\frac{1}{\dot{m}_{\mathrm{hf}}C_{\mathrm{hf}}}+\frac{1}{\dot{m}_{\mathrm{cf}}C_{\mathrm{cf}}}\right)\mathrm{d}A \quad (5)$$

was integrated to produce

$$\ln\left(\frac{T_{\mathrm{h2}}-T_{\mathrm{c2}}}{T_{\mathrm{h1}}-T_{\mathrm{c1}}}\right) = -UA\left(\frac{1}{\dot{m}_{\mathrm{hf}}C_{\mathrm{hf}}}+\frac{1}{\dot{m}_{\mathrm{cf}}C_{\mathrm{cf}}}\right). \quad (6)$$

One of the basic assumptions in the LMTD method is that the flow thermal capacity of the test fluid (i.e. $\dot{m}_{\mathrm{h}}C_{\mathrm{h}}$ or $\dot{m}_{\mathrm{c}}C_{\mathrm{c}}$) is constant both in hot and cold side fluids along the flow direction. When there is a phase change on one side, the thermal capacity includes the latent heat of phase change, which will be much greater than the original thermal capacity of the fluid, and can be represented by the effective thermal capacity in equation (3). Therefore, the LMTD method already implicitly includes the assumption of this constant effective thermal capacity.

Another important assumption in deriving the log-mean-temperature-difference (LMTD) is that the overall heat transfer coefficient is constant along the flow direction in the heat exchanger. However, neither the local heat transfer coefficient nor the thermal capacity is constant in a phase-change slurry flow, a fact which makes it difficult to use the LMTD method. Therefore, this study measured friction and heat transfer coefficients locally (instead of measuring inlet and outlet temperatures only) in the analysis of the PCM slurry flow.

The results described above suggest the following question: why did Cleary *et al.* [1] obtain a small increase, or sometimes a decrease in the convective heat transfer coefficient when the ice-slurry was used?

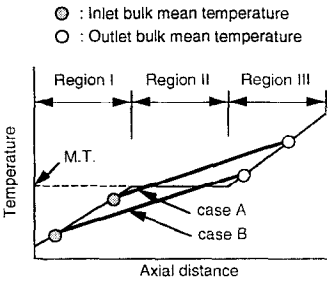

FIG. 9. Possible bulk mean temperature profile and inlet and outlet temperatures for the experiment of Cleary *et al.* [1].

A possible reason can be found in Fig. 9. If the inlet and outlet temperatures were represented by Case A, the overall heat transfer coefficient would be overestimated. If they were represented by Case B, it would be underestimated.

CONCLUSIONS

A long heating test section (627 diameters) with a uniform heat flux boundary condition was constructed in order to study the effect of phase-change phenomena of a phase-change-material (PCM)–water slurry on the convective heat transfer coefficient in turbulent flow. The major finding in the present study concerns the advantages of a three-region melting model, which was proposed to estimate the bulk mean temperature of a mixture of fine PCM particles and water, and to analyze experimental data for a two-phase liquid–solid mixture. A sudden change of pressure took place at the point where melting of the PCM particles occurred. At this point, the bulk mean temperature of the mixture reached the melting temperature of the PCM. The other findings are briefly listed below:

1. A new technique to generate very fine PCM particles inside a flow loop using an emulsifier was introduced. The size of the PCM particles was approximately 0.1 mm, which was small enough to prevent clogging in the flow loop.
2. A 10% suspension of solid hexadecane particles in water has approximately a 13% higher pressure drop than a 10% emulsion of liquid hexadecane in water. This was used to locate the melting of the PCM particles.
3. Both the local convective heat transfer coefficient and the effective thermal capacity of a phase-change-material slurry varied significantly along the heating test section; these phenomena made the LMTD method difficult to use for the analysis of convective heat transfer with a two-phase liquid–solid mixture.
4. The local convective heat transfer coefficient increased in the region where the bulk mean temperature was below the melting temperature of the PCM (Region I), decreased sharply where phase change occurred (Region II), and increased again

slightly further downstream (Region III). It is hypothesized that in Region I there is a thin layer of melted suspension, which grew abruptly in Region II; no solid particles existed in Region III.

Acknowledgement—This work was supported by the U.S. Department of Energy, Office of Conservation and Renewable Energy, whose support is gratefully acknowledged.

REFERENCES

1. C. Cleary, S. Day, R. Lindsay, C. Murry, R. Gupta, B. Larkin, H. Thompson, M. Wiggin and J. S. O'C. Young, Hydraulic characteristics of ice slurry and chilled water flows. In *IEA District Heating: Advanced Energy Transmission Fluids—Final Report of Research*. Novem BV, Sittard, Netherlands (1990).
2. P. J. Winters, Phase two laboratory testing of direct freeze ice slurry district cooling. Project final report, prepared by CBI Industries, Inc., for the U.S. Department of Energy, DOE Contract No. DE-FG01-88CE26559 (1991).
3. G. Lane, *Solar Heat Storage: Latent Heat Materials* (Edited by G. Lane), vol. II. CRC Press, Cleveland (1986).
4. K. E. Kasza and M. M. Chen, Improvement of the performance of solar energy or waste heat utilization systems by using phase-change slurry as an enhanced heat-transfer storage fluid, *J. Solar Energy Engng* **107**, 229–236 (1985).
5. J. P. Holman, *Heat Transfer* (5th Edn). McGraw-Hill, New York (1981).
6. C. W. Sohn and M. M. Chen, Microconvective thermal conductivity in disperse two-phase mixtures as observed in a low velocity Couette flow experiment, *J. Heat Transfer* **103**, 47–51 (1981).
7. C. W. Sohn and M. M. Chen, Heat transfer enhancement in laminar slurry pipe flows with power law thermal conductivities, *J. Heat Transfer* **106**, 539–542 (1984).
8. D. P. Colvin, J. C. Mulligan and Y. G. Bryant, Enhanced heat transfer in environmental systems using microencapsulated phase change materials, *22nd International Conference on Environmental Systems* (1992).
9. S. K. Roy and S. Sengupta, The melting process within spherical enclosures, *J. Heat Transfer* **109**, 460–462 (1987).
10. P. Charunyakorn, S. Sengupta and S. K. Roy, Forced convection heat transfer in microencapsulated phase change material slurries: flow in circular ducts, *Int. J. Heat Mass Transfer* **34**, 819–833 (1991).
11. S. K. Roy and S. Sengupta, An evaluation of phase change microcapsules for use in enhanced heat transfer fluids, *Int. Comm. Heat Mass Transfer* **18**, 495–507 (1991).
12. D. P. Colvin and J. C. Mulligan, Thermal energy storage apparatus using enhanced phase change material, U.S. Patent 4,807,696 (1989).
13. D. P. Colvin and J. C. Mulligan, Method of using a PCM slurry to enhance heat transfer in liquids, U.S. Patent 4,911,232 (1990).
14. E. Choi, Y. I. Cho and H. G. Lorsch, Effects of emulsifier on particle size of a PCM in a mixture with water, *Int. Comm. Heat Mass Transfer* **18**, 759–766 (1991).
15. R. W. Allen and E. R. G. Eckert, Friction and heat-transfer measurements to turbulent pipe flow of water ($Pr = 7$ and 8) at uniform wall heat flux, *J. Heat Transfer* **86**, 301–310 (1964).
16. R. W. Allen, Measurements of friction and local heat transfer for turbulent flow of a variable property fluid (water) in a uniformly heated tube, Ph.D. Thesis, University of Minnesota (1959).
17. J. P. Hartnett, Experimental determination of the thermal entrance length for the flow of water and of oil in circular pipes, *J. Heat Transfer* **77**, 1211–1220 (1955).
18. E. Choi, Forced convection heat transfer with water and phase-change-material slurries: turbulent flow in a circular tube, Ph.D. Thesis, Drexel University (1993).
19. W. M. Kays and M. E. Crawford, *Convective Heat and Mass Transfer* (2nd Edn), pp. 196–199. McGraw-Hill, New York (1980).
20. B. S. Petukhov, Heat transfer and friction in turbulent pipe flow with variable physical properties, *Adv. Heat Transfer* **6**, 503–564 (1970).
21. F. W. Dittus and L. M. K. Boelter, Heat transfer in automobile radiators of the tubular type, *Univ. Calif. Publ. Engng* **2**, 443–461 (1930).
22. E. Choi, Y. I. Cho and H. G. Lorsch, Thermal analysis of the mixture of laboratory and commercial grades hexadecane and tetradecane, *Int. Comm. Heat Mass Transfer* **19**, 1–15 (1992).